Geophys. J. Int. (2001) **147,** 579–589

Modelling of viscoelastic plume–lithosphere interaction using the adaptive multilevel wavelet collocation method

Oleg V. Vasilyev,[1] Yuri Yu. Podladchikov[2] and David A. Yuen[3]

[1] *Department of Mechanical and Aerospace Engineering, University of Missouri-Columbia, Columbia,* MO 65211, *USA. E-mail: VasilyevO@missouri.edu*
[2] *Geologisches Institut, ETH-Zurich, Sonneggstrasse* 5, CH 8092, *Zurich, Switzerland. E-mail: yura@erdw.ethz.ch*
[3] *Minnesota Supercomputing Institute and Department of Geology and Geophysics, University of Minnesota, Minneapolis,* MN 55415, *USA. E-mail: davey@krissy.msi.umn.edu*

Accepted 2001 June 29. Received 2001 May 10; in original form 2000 March 30

SUMMARY

Modelling of mantle flows with sharp viscosity contrasts in a viscoelastic medium is a challenging computational problem in geodynamics because of its multiple-scale nature in space and time. We have employed a recently developed adaptive multilevel wavelet collocation algorithm to study the dynamics of a small rising diapir interacting with a stiff lithosphere in a Maxwell viscoelastic mantle. In this kinematic model we have prescribed the upward velocity of the diapir and then we need to integrate in time only the momentum equation governing the temporal evolution of the pressure, stress and velocity components, which together constitute a sixth-order system in time. The total number of collocation points did not exceed 10^4, compared to more than 10^6 gridpoints using conventional evenly spaced grid methods. The viscosity of the diapir is 10^{-4} times lower than that of the surrounding mantle, while the viscosity of the thin lithosphere, about 5–10 per cent of the entire layer depth, is 10^4–10^8 times stiffer than the ambient mantle. Our results demonstrate the efficacy of wavelets to capture the sharp gradients of the stress and pressure fields developed in the diapiric impingement process. The interaction of the viscoelastic lithosphere with the rising viscoelastic diapir results in the localization of stress within the lithosphere. The magnitude of the stress fields can reach around 100–300 MPa. Our simple kinematic model shows clearly that viscoelasticity can potentially play an important role in the dynamics of the lithosphere, especially concerning the potential severage of the lithosphere by mantle upwellings.

Key words: diapirs, geodynamics, lithosphere, numerical methods, viscoelasticity, wavelets.

1 INTRODUCTION

There has been a growing recognition of the important role played by viscoelasticity in mantle flow processes since the pioneering work of Harder (1991). Ricard *et al.* (1993) have attempted to model finite amplitude subduction processes with viscoelastic normal modes, and recently Toth & Gurnis (1998) have studied the initiation of subduction with the finite element method. Kameyama *et al.* (1999) have investigated the thermomechanical evolution of viscoelastic shear zones, and Schmalholz & Podladchikov (1999) and Schmalholz *et al.* (2001) have studied the folding and buckling of viscoelastic media in the large-amplitude regime. Poliakov *et al.* (1993) have investigated diapiric upwelling within a viscoelastic lithosphere using a finite difference method. The modelling of viscoelastic flows in geodynamics remains a very difficult problem because of both theoretical and numerical difficulties. The fundamental problem in modelling time-dependent viscoelastic flows is the mixed rheological properties, which result in a time dependence of the stress on the history of the forcing function. The advection and rotation of stress fields are also important in problems with free surfaces and faulting. Some finite element models of viscoelastic behaviour have been developed by Melosh & Raefsky (1980) for a fluid with a non-Newtonian viscous rheology and by Chery *et al.* (1991) for coupled viscoelastic and plastic rheologies. Both approaches are very powerful, but they can simulate only relatively small deformations and are limited by distortion of the Lagrangian grid. Therefore, it is important to

consider new non-traditional methods for modelling complex rheologies over long timespans that are adaptive in nature for capturing moving fronts involving sharp gradients in the viscosity and stress fields. In this paper we introduce the adaptive wavelet collocation method to study a model geophysical problem of a low-viscosity diapir impinging on a highly viscous thin lithosphere in a viscoelastic mantle. This model illustrates the fundamentals of the dynamics of this prototype geodynamic process and the ability of the wavelet collocation method to simulate it numerically.

Traditional methods used for numerical solutions of geophysical problems mostly fall into three classes: finite difference and finite volume methods, finite element methods, and spectral methods. The advantages of using either finite difference, finite volume or finite element methods are simplicity in adapting to complex geometries and sparseness of the resulting matrices, while the basic advantage of spectral methods lies in the exponential rate of convergence.

If the solution of a geophysical problem has regular features, any of these numerical techniques can be applied. However, in many problems of geophysics there exist a multiplicity of very different spatial and temporal scales in the solution, as in strongly time-dependent non-Newtonian convection (Malevsky & Yuen 1992), plume–lithosphere interaction (Larsen *et al.* 1993; Christensen & Ribe 1994), and diapir–elastic crust interaction (Poliakov *et al.* 1993). This particular attribute of multiple spatial scales, which possibly change over time, will put great strain on the aforementioned methods. Spectral methods would have some problems capturing large irregularities of the solutions. Accurate representation of the solution in regions where sharp physical transitions occur will require the implementation of dynamically adaptive finite difference or finite element methods (e.g. Braun & Sambridge 1994). Kameyama *et al.* (1999) employed an adaptive finite difference method in a 1-D model but still needed 10 000 points to resolve sharp shear zones being shrunk by viscous heating. Schmalholz *et al.* (2001) developed a hybrid finite difference spectral method in two dimensions and found that 1000 points in the vertical are required in the large-strain, $O(1)$, regime. In these methods an automatic error estimation step should be employed to determine locally the accuracy of the solution. The main difficulties of existing adaptive methods are finding stable accurate spatial operators at the interface of computational molecules of very different sizes and developing a computationally efficient robust adaptive procedure, which would dynamically adapt the computational grid to local structures of the solution. Similar numerical problems associated with large-strain treatment of heterogeneous viscoelastic material are well known in computational fluid mechanics and several areas of applications such as polymer processing (Keunings 2001).

Wavelet analysis is a new numerical concept that allows one to represent a function as a linear combination of building blocks (a basis), called wavelets, which are localized in both *location* and *scale* (Daubechies 1992; Louis *et al.* 1997; Meyer 1992; Strang & Nguyen 1996). Good wavelet localization properties in physical and wavenumber spaces are to be contrasted with the spectral approach, which employs infinitely differentiable functions but with global support and small discrete changes in the resolution. On the other hand, finite difference, finite volume and finite element methods have small compact support but poor continuity properties. Consequently, spectral methods have good spectral localization (which results in exponential convergence rates), but poor spatial localization (which results in Gibbs phenomena in regions of fast transitions), while finite difference, finite volume and finite element methods have good spatial localization but poor spectral localization (which results in algebraic convergence rates). Wavelets appear to combine the advantages of both spectral and finite difference bases. One of the principal purposes of this paper is to present the essence of the wavelet method, to provide sufficient details for its implementation and to demonstrate its prowess in solving geophysical problems with a localization of physical properties and computational economy in doing so.

The paper is organized as follows. In Section 2 we present in detail the mathematical formulation of the model problem involving a low-viscosity diapir impinging on a highly viscous thin lithosphere in a viscoelastic mantle. Numerical implementation of the adaptive wavelet collocation algorithm is described in Section 3. In Section 4 we discuss the time-dependent results of the viscoelastic flow for the model problem described in Section 2. Finally, the geophysical implications and conclusions concerning the role of viscoelastic flow in the mantle are given in Section 5.

2 MATHEMATICAL MODEL

We consider a plane-strain viscoelastic flow in the mantle with a strongly variable viscosity driven by density inhomogeneities in a vertical rectangular domain $[0, L^*]\times[0, L^*]$. L^* can be considered to have the dimension of the upper mantle. The asterisk denotes dimensional quantities. Our model viscoelastic mantle consists of a thin, highly viscous upper boundary layer (lithosphere) that interacts with a highly variable viscous interior (the mantle) associated with a rising diapir, which is modelled kinematically by a vertically rising, small, lower-density sphere with a viscosity considerably lower than that of the ambient mantle.

This viscoelastic model problem involves six unknowns [two velocity components, V_1^* and V_2^*, pressure, p^* (the isotropic part of the 3-D stress tensor with a minus sign), and three in-plane deviatoric components of the stress tensor, τ_{11}^*, τ_{22}^* and τ_{12}^*]. The dimensional scales are the size of the domain L^*, the dynamic viscosity μ^*, the shear elastic modulus G^* and the gravity force per unit volume $\rho^* g^*$, where ρ^* is the characteristic scale for the density deviations and g^* is the gravity acceleration. We emphasize that both pressure p^* and density ρ^* are the deviations from the reference hydrostatic state. There is also an extra parameter, the 'inertial density', ρ_i^*, which may not be equal to ρ^* (Poliakov *et al.* 1993). The three independent characteristic scales used in dimensional analyses are L^*, μ^* and $\rho^* g^*$, which makes the stress, time and velocity scales $\rho^* g^* L^*$, $\mu^*/(\rho^* g^* L^*)$ and $[\rho^* g^* (L^*)^2]/\mu^*$, respectively. Finite amplitude effects of stress advection have not been included.

The viscoelastic equations describing the conservation of momentum, mass and viscoelastic constitutive relationship are given respectively by

$$\frac{dV_i}{dt} = \frac{1}{Re}\left[-\frac{\partial p}{\partial x_i} + \frac{\partial \tau_{ij}}{\partial x_j} + \rho e_{gi}\right], \tag{1}$$

$$\frac{\partial p}{\partial t} = -\frac{K}{De}\frac{\partial V_i}{\partial x_i}, \tag{2}$$

$$\frac{D\tau_{ij}}{Dt} = \frac{2}{De}\left[-\frac{\tau_{ij}}{2\mu} + \frac{1}{2}\left(\frac{\partial V_i}{\partial x_j} + \frac{\partial V_j}{\partial x_i}\right) - \frac{1}{3}\frac{\partial V_k}{\partial x_k}\delta_{ij}\right], \tag{3}$$

where $i, j, k = 1, 2$, repeated indices imply summation, δ_{ij} is the Kronecker delta and $e_{gi} = (0, -1)$ is the unity vector in the direction of gravitational acceleration. The substantial time derivative dV_i/dt and the upper convective objective stress rate $D\tau_{ij}/Dt$ (Huilgol & Phan-Thien 1997) are given by

$$\frac{dV_i}{dt} = \frac{\partial V_i}{\partial t} + V_k \frac{\partial V_i}{\partial x_k}, \tag{4}$$

$$\frac{D\tau_{ij}}{Dt} = \frac{\partial \tau_{ij}}{\partial t} + V_k \frac{\partial \tau_{ij}}{\partial x_k} - \tau_{kj} \frac{\partial V_i}{\partial x_k} - \tau_{ik} \frac{\partial V_j}{\partial x_k}, \tag{5}$$

respectively. The three independent dimensionless parameters appearing in the equations are

$$Re = \frac{\rho_i^* \rho^* g^* (L^*)^3}{(\mu^*)^2}, \quad De = \frac{\rho^* g^* L^*}{G^*}, \quad K = \frac{K^*}{G^*}. \tag{6}$$

These parameters represent the Reynolds and Deborah numbers, and the measure of the ratio of bulk, K^*, and shear, G^*, elastic moduli. The Deborah number is the ratio of the Maxwell relaxation time μ^*/G^* to the characteristic timescale defined above.

The Deborah number De (Reiner 1964) is a measure of the relative influence of the viscous versus elastic deformation modes, such that when $De = O(1)$ both modes are comparable, while $De \to 0$ and $De \to \infty$ respectively represent the viscous and elastic limits. For realistic Earth parameters, De may lie between 10^{-2} and 10^{2} with corresponding timescales between 10^{-1} and 10^{2} Myr and spatial scales between 5 and 500 km (Vasilyev *et al.* 1997b). Note that although eqs (1)–(3) can be rescaled to have only two independent dimensional parameters, we have chosen this form for geophysical relevance.

The density perturbation provides the source term for driving the viscoelastic flow. The non-dimensional density perturbation ρ in eq. (1) is chosen to be

$$\rho(x_1, x_2, t) = -f_0(x_1, x_2, t), \tag{7}$$

where

$$f_0(x_1, x_2, t) = \exp\left[-\frac{(x_1 - x_{10})^2 + [x_2 - x_{20} - v_{20}(t - t_0)]^2}{r_0^2}\right], \tag{8}$$

v_{20} is the speed with which the diapir rises and (x_{10}, x_{20}) is the diapir location at the initial time t_0.

The non-dimensional viscosity μ is taken to be

$$\mu(x_1, x_2) = [\mu_0 + (\mu_1 - \mu_0) f_1(x_2)][1 - f_0(x_1, x_2, t)] + \mu_2 f_0(x_1, x_2, t), \tag{9}$$

where

$$f_1(x_2) = \exp\left[-\frac{(x_2 - 1)^2}{\lambda^2}\right]. \tag{10}$$

Constants μ_0, μ_1, μ_2, λ, r_0 and v_{02} and functions f_1 and f_2 are chosen in such a way that the high-viscosity region is concentrated near the top. The problem is solved for five different cases. The following parameters are common for all cases: $Re = 10^{-3}$, $De = 10^{-2}$, $K = 1$, $\mu_0 = 1$, $r_0 = 0.05$, $(x_{10}, x_{20}) = (0.6, 0.6)$, while parameters μ_1, μ_2, λ and v_{02} are varied. Five sets of parameters corresponding to different cases are given in Table 1. These parameters are chosen so that they allow for the effect of the large viscosity contrast (μ_1, μ_2), the influence of the lithosphere thickness (λ) and viscoelastic memory effects (v_{02}).

Table 1. The parameters for the five different cases studied.

	Case I	Case II	Case III	Case IV	Case V
μ_1	10^4	10^4	10^4	10^8	10^4
μ_2	10^{-2}	10^{-2}	10^{-2}	10^{-4}	10^{-2}
λ	2×10^{-2}	2×10^{-2}	5×10^{-3}	2×10^{-2}	2×10^{-2}
v_{02}	$4 \times 10^{-2}/De$	$10^{-1}/De$	$10^{-1}/De$	$10^{-1}/De$	0

The initial and boundary conditions are respectively given by

$$V_i(x_1, x_2, 0) = p(x_1, x_2, 0) = \tau_{ij}(x_1, x_2, 0) = 0, \quad i, j = 1, 2, \tag{11}$$

and

$$V_1(0, x_2, t) = V_1(1, x_2, t) = V_2(x_1, 0, t) = V_2(x_1, 1, t) = 0, \tag{12}$$

$$\tau_{12}(x_1, 0, t) = \tau_{12}(x_1, 1, t) = \tau_{12}(0, x_2, t) = \tau_{12}(1, x_2, t) = 0. \tag{13}$$

In order to illustrate the elastic nature of the solution, we consider additional Case V, where the initial condition is taken to be the solution of Case I at time $t = 3.0De$ and the diapir velocity is set to zero. This time is long enough so that the solution shows viscoelastic memory effect. Further integration in time results in viscous relaxation and allows the comparison of the solution with the elastic case, that is, when the diapir continues moving.

This particular set of parameters and boundary conditions is intentionally chosen to ensure that the non-linear terms in eqs (1) and (3) defining convective derivatives in our model problem can be neglected. Despite the fact that non-linearities certainly play an important role in many geophysical applications, their treatment is beyond the scope of this paper. Moreover, many geophysical applications up to now have neglected these non-linear terms in stress advection, e.g. Toth & Gurnis (1998). The primary objective of this paper is to demonstrate the ability of the wavelet numerical algorithm to resolve a great range of spatial scales and to handle the large viscosity contrasts, which are the two major numerical challenges in geodynamic modelling.

It should be noted that the model problem is different from the one described in Vasilyev *et al.* (1997b). In particular, the model described in this section is aimed at mimicking the dynamics of a small rising diapir interacting with a stiff lithosphere in a Maxwell viscoelastic mantle, while in Vasilyev *et al.* (1997b) we focused our attention on viscoelastic contrasts interacting with a global density forcing.

3 NUMERICAL METHOD

In this section we describe the basic elements of the dynamically adaptive wavelet collocation method used for this viscoelastic model problem. For simplicity of presentation we formulate the algorithm for a 2-D problem. The generalization of the algorithm into three dimensions is straightforward. In describing

the method we try to present it in a way that is easy to understand and implement without deep knowledge of wavelet theory. For theorem proofs and other mathematical aspects of the algorithm we refer to the articles of Vasilyev & Paolucci (1996,1997), Vasilyev *et al.* (1997a), Vasilyev & Bowman (2000) and Vasilyev (1996, 2001).

3.1 Multilevel wavelet approximation

Wavelets are constructed by the discrete (typically dyadic) dilation $a_j = a_0 2^{-j}$ and translation $b_k^j = a_j k$ of a single function, called the 'mother' wavelet, $\psi(x)$, which has good localization properties in physical as well as wavenumber spaces. Examples of 'mother' wavelets are shown in Fig. 1. The discrete dilations and translations generate a doubly indexed set of wavelet functions $\psi_k^j(x)$ given by

$$\psi_k^j(x) = a_j^{-1/2} \psi\left(\frac{x - b_k^j}{a_j}\right). \tag{14}$$

Each of the functions $\psi_k^j(x)$ is a wavelet of scale a_j located at position b_k^j. For notational convenience we use the superscript to denote the level of resolution and the subscript to denote the location in physical space (with the exception of a_j). The wavelet decomposition of a 1-D function $u(x)$ may be written as

$$u(x) = \sum_{j=0}^{\infty} \sum_{k \in Z} c_k^j \psi_k^j(x). \tag{15}$$

In other words, wavelet decomposition can be viewed as multilevel or multiresolution representation of a function, where each level of resolution consists of wavelets having the same scale a_j but different locations b_k^j. For details of wavelet theory we refer to the following books: Daubechies (1992), Louis *et al.* (1997), Meyer (1992) and Strang & Nguyen (1996).

The more familiar trigonometric decompositions of a periodic function can be expressed using the above notation as

$$u(x) = \sum_{j=0}^{+\infty} \sum_{k=0}^{1} c_k^j \sin[j(x + \pi k/2)], \tag{16}$$

where j corresponds to the frequency (the scale) of the basis function and k describes its location. In this particular example there are only two locations of the basis function, which is due to the global support of the basis function.

Wavelet decompositions can be introduced in the same way in two dimensions. In this paper we construct a 2-D wavelet basis as a tensor product of two 1-D bases:

$$\psi_{k,l}^j(x, y) = \psi_k^j(x) \psi_l^j(y), \tag{17}$$

where $\psi_k^j(x)$ and $\psi_l^j(y)$ are two 1-D wavelets. Therefore, a function $u(x, y)$, defined in rectangular domain $\Omega = [X_1, X_2] \times [Y_1, Y_2]$, is approximated as a linear combination of basis functions (eq. 17) and is given by

$$u^J(x, y) = \sum_{j=0}^{J} \sum_{(k,l) \in Z^2} c_{k,l}^j \psi_{k,l}^j(x, y). \tag{18}$$

After discretization of this rectangular domain the scales and locations are defined by

$$\begin{aligned} &a_{xj} = 2^{-j_x} a_{x0}, \quad b_{xk}^j = \frac{X_1 + X_2}{2} + a_{xj} k, \\ &a_{x0} = 2^{-L_x}(X_2 - X_1), \quad j_x = 1, 2, \ldots, J_x \end{aligned} \tag{19}$$

and

$$\begin{aligned} &a_{yj} = 2^{-j_y} a_{y0}, \quad b_{yl}^j = \frac{Y_1 + Y_2}{2} + a_{yj} l, \\ &a_{y0} = 2^{-L_y}(Y_2 - Y_1), \quad j_y = 1, 2, \ldots, J_y. \end{aligned} \tag{20}$$

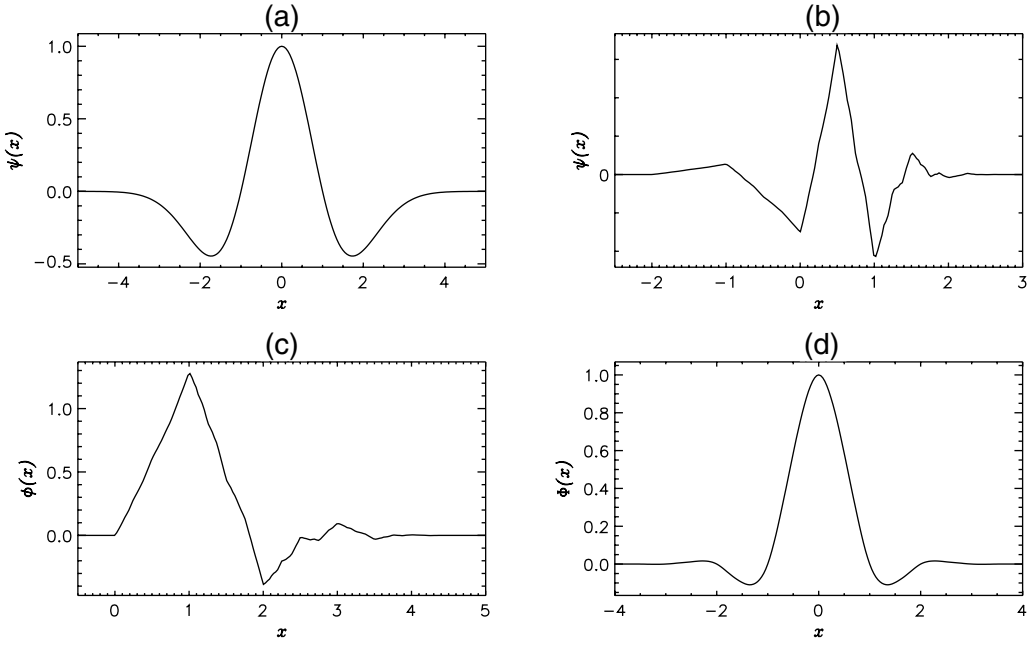

Figure 1. Examples of wavelets and scaling functions: (a) Mexican hat wavelet, (b) Daubechies wavelet of order 3, (c) Daubechies scaling function of order 3, and (d) cardinal interpolating wavelet of order 6.

For clarity of presentation we use subscripts x and y to denote all the parameters associated with directions x and y respectively. Integer parameters L_x and L_y determine the largest scales of the approximation in the x- and y-directions, while integers J_x and J_y define the finest scales of the approximation (18).

For clarity of discussion, all wavelets whose centres are located within the rectangular domain will be called internal wavelets; the other wavelets will be called external wavelets. Due to the local or approximately local (exponential decay) support of a wavelet, only those external wavelets that are located close to the boundary contribute to the approximation $u^J(x, y)$. Thus wavelets that are located far from the domain can be omitted from the approximation (18). On each side of the computational domain we will keep only N_x and N_y external wavelets in the directions x and y respectively. Then the approximation (18) can be rewritten as

$$u^J(x, y) = \sum_{j=0}^{J} \sum_{(k,l)=Z_{xy}^j} c_{k,l}^j \psi_{k,l}^j(x, y)\,, \tag{21}$$

where $Z_{xy}^j = [-K_x^j, K_x^j] \times [-K_y^j, K_y^j]$, $K_x^j = 2^{L_x+j_x-1} + N_x$ and $K_y^j = 2^{L_y+j_y-1} + N_y$.

3.2 Wavelet interpolation

The approximation (21) can be considered as a wavelet interpolation provided there is a way to obtain values of wavelet coefficients from the values of the function at a discrete set of grid (collocation) points. Due to the multilevel character of approximation (21) we choose the set of collocation points in such a way that any finer level contains the collocation points of the coarser-level functions. This relation between collocation points of different levels of resolution enables us to have the same values of the function at different levels of resolution at the same collocation points.

We associate each wavelet with one particular collocation point. Note that wavelets at different levels of resolution may have the same collocation point. For internal wavelets we chose wavelet locations (b_{xk}^j, b_{yl}^j) to be the collocation points (x_k^j, y_l^j). The collocation points of external wavelets are taken to correspond to the locations of internal wavelets of a finer level of resolution. For example, if we let $b_{xk}^j < X_1$ and $Y_1 < b_{yl}^j < Y_2$, then the collocation point is taken to be $(x_k^j, y_l^j) = (b_{xk_1}^{j_1}, b_{yl}^j)$, where $j_1 = j + [\log_2(N_x)] + 1$ ([.] indicates the integer part) and $(b_{xk_1}^{j_1} - X_1)/a_{xj_1} = (X_1 - b_{xk}^j)/a_{xj}$.

Wavelet coefficient are found in two steps:

(i) *Initialization step.* At the coarsest level of resolution ($j = 0$) we set the values of the approximation at collocation points (x_k^0, y_l^0) equal to the values of the function at these locations. Then, in order to obtain wavelet coefficients $c_{k,l}^0$, we solve the following linear system of equations:

$$u^J(x_k^0, y_l^0) = \sum_{(m,n)\in Z_{xy}^0} c_{m,n}^0 \psi_{m,n}^j(x_k^0, y_l^0)\,. \tag{22}$$

(ii) *Recursion step.* For each level of resolution $0 < j \le J$ we fix the values of wavelet coefficients at the lower levels of resolution. Then we form the residual $\Delta^j(x_k^J, y_l^J)$ between values of a function at collocation points of the finest level of resolution and the wavelet approximation at the previous level of resolution,

$$\Delta^j(x_k^J, y_l^J) = u^J(x_k^J, y_l^J) - \sum_{s=0}^{j-1} \sum_{(m,n)\in Z_{xy}^s} c_{m,n}^s \psi_{m,n}^s(x_k^J, y_l^J)\,. \tag{23}$$

Then we set the values of the individual contribution of the jth level of resolution at collocation points (x_k^j, y_l^j) equal to values of the residual $\Delta^j(x_k^j, y_l^j)$ at these locations. Thus in order to obtain wavelet coefficients $c_{k,l}^j$ we solve the following linear system of equations:

$$\Delta^j(x_k^j, y_l^j) = \sum_{(m,n)\in Z_{xy}^j} c_{m,n}^j \psi_{m,n}^j(x_k^j, y_l^j)\,. \tag{24}$$

In other words, wavelet coefficients are found in this recursive manner. We start from the coarsest level of resolution and progressively move to the finest level. At each level of resolution the coefficients of the lower levels are fixed, so we only obtain the coefficients corresponding to that level.

In actual implementation of the algorithm the values of the residual $\Delta^j(x_k^j, y_l^j)$, $(k, l) \in Z_{xy}^j$, are found recursively by using the following relation:

$$\Delta^j(x_k^J, y_l^J) = \begin{cases} \Delta^{j-1}(x_k^J, y_l^J) - \displaystyle\sum_{(m,n)\in Z_{xy}^{j-1}} c_{m,n}^{j-1} \psi_{m,n}^{j-1}(x_k^J, y_l^J) & 1 \le j \le J \\ u^J(x_k^J, y_l^J) & j = 0 \end{cases}, \tag{25}$$

The solution of eqs (22) and (24) for a general wavelet might be expensive. In order to make the algorithm computationally efficient we utilize cardinal interpolating wavelets (Donoho 1992; Sweldens & Schröder 1996). By cardinal wavelets we mean wavelets that satisfy the following relation:

$$\psi(k) = \delta_{k,0}\,, \tag{26}$$

where $\delta_{i,k}$ is the Kronecker delta symbol. An example of such a cardinal scaling function is shown in Fig. 1(d).

The procedure of finding wavelet coefficients is as follows. First we find coefficients for internal wavelets, then we find c coefficient for all external wavelets except corner wavelets, and finally we find coefficients for corner wavelets. This three-step approach enables us to find wavelet coefficients without matrix inversion. The cost of finding wavelet coefficient at the jth level of resolution is N^j, where N^j is the number of wavelets at the jth level of resolution.

Knowing the values of wavelet coefficients, the function $u(x, y)$ can be approximated by eq. (21). The derivatives $u^{(m,n)}(x, y)$ of a function are approximated by differentiating eq. (21), where $m, n = 0, 1$. Thus the derivative of a function $u(x, y)$ is found using the following relation:

$$u^{(m,n)}(x, y) = \sum_{j=0}^{J} \sum_{k\in Z_x^j} \sum_{l\in Z_y^j} c_{k,l}^j \psi_{k,l}^{j(m,n)}(x, y)\,. \tag{27}$$

Derivatives higher than first order can be found by consecutive applications of the above algorithm.

3.3 Wavelet compression

The absolute value of the wavelet coefficient $c^j_{k,l}$ appearing in approximation (21) depends upon the local regularity of $u(x, y)$ in the neighbourhood of location (b^j_{xk}, b^j_{yl}). A good approximation of a function is retained even when wavelets whose coefficients are below a prescribed threshold parameter ε are omitted and only those wavelets are kept whose coefficients are above the threshold. In other words, $u(x, y)$ can be approximated by

$$u^J_{\geq}(x, y) = \sum_{j=0}^{J} \sum_{(k,l)\in Z^j_{xy\geq}} c^j_{k,l}\psi^j_{k,l}(x, y)\,, \tag{28}$$

where the 2-D integer set $Z^j_{xy\geq}$ consists of wavelets whose amplitudes satisfy the following inequality:

$$\left|c^j_{k,l}\right| \geq a^{1/2}_{xj} a^{1/2}_{yj}\varepsilon\,. \tag{29}$$

We also define the 2-D integer set $Z_{xy\geq}$ is such a way that collocation points (x^J_k, y^J_l), $(k, l)\in Z_{xy\geq}$ at the finest level of resolution are constructed as a union of collocation points at all levels of resolution. It is easy to show that

$$\left\|u^J(x, y) - u^J_{\geq}(x, y)\right\|_{L^2(R^n)} \leq C\varepsilon\left\|u^J(x, y)\right\|_{L^2(\Omega)}\,, \tag{30}$$

where C is a constant of order unity. In Fig. 2 we sketch the locations of wavelets used in a four-level approximation of a 1-D function. Fig. 2 also shows schematically the locations of wavelets whose coefficients are above a given threshold parameter for a function that has a sharp transition in the middle of the domain. This example illustrates the considerable savings one can achieve by keeping in the approximation only significant wavelets and omitting those that play an insignificant role in the approximation.

The derivatives $u^{(m,n)}(x, y)$ of a function are approximated by differentiating eq. (28) and are given by

$$u^{J(m,n)}_{\geq}(x, y) = \sum_{j=0}^{J} \sum_{(k,l)\in Z^j_{xy\geq}} c^j_{k,l}\psi^{j(m,n)}_{k,l}(x, y)\,. \tag{31}$$

For convenience of discussion, all wavelets $\psi^j_{k,l}$ whose coefficients satisfy inequality (29) will be called active wavelets. Thus the set $Z^j_{xy\geq}$ consists of indexes of active wavelets of the jth level of resolution.

Note that if function $u(x, y)$ has localized structures, then approximation (28) has considerably fewer wavelets then approximation (21). We also note that the accuracy of the approximation is controlled by ε: the smaller the value of epsilon, the closer the approximation is to $u^J(x, y)$.

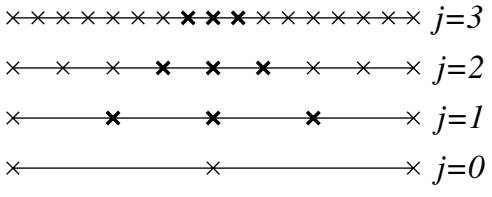

Figure 2. Locations of wavelets (×) used in the approximation of a function with four levels of resolution ($j=0, \ldots, 3$), where bold symbols denote wavelets whose coefficients are above a given threshold ε in the approximation of a function with a sharp transition.

3.4 Fast wavelet collocation transform

In the application of partial differential equations it is essential to find values of the derivative of a function at collocation points by providing values of the function at the same collocation points. This can be achieved by means of the fast wavelet collocation transform (FWCT). The essential ingredients of the FWCT are described in Section 3.2. Assuming that locations of active wavelets are prescribed *a priori*, the FWCT consists of two steps.

(i) Given values of a function at collocation points (x^J_k, y^J_l) $(k, l)\in Z_{xy\geq}$ we find values of wavelet coefficients at all levels of resolution. The procedure is the same as that described in Section 3.2. We start from the coarsest level of resolution and progressively move to the finest level. At each level of resolution j, the coefficients of the lower levels are fixed, so we only obtain the coefficients $c^j_{k,l}$, $(k, l)\in Z^j_{xy\geq}$ corresponding to that level of resolution.

(ii) Values of the derivative of a function are found by evaluating eq. (28) at (x^J_k, y^J_l) $(k, l)\in Z_{xy\geq}$ collocation points.

Due to the fact that the wavelet function has compact or effectively compact support, the overall computational cost of finding wavelet coefficients and values of the derivatives of a function at collocation points is $O((J+1)M^2\mathcal{N})$, where $\mathcal{N}$ is the total number of collocation points and M is the wavelet support. Thus the smaller the wavelet support, the less expansive it is to evaluate the derivatives of the function given its values at collocation points.

3.5 Application to partial differential equations

Let us discuss the application of wavelet interpolation and compression algorithms to the numerical solution of partial differential equations. We focus on evolutionary equations that can be applied in geophysics. The most general form of a system of partial differential equations can be written as follows:

$$\mathbf{F}\left(\frac{\partial \mathbf{u}}{\partial t}, \mathbf{u}, \nabla\mathbf{u}, \mathbf{x}, t\right) = 0\,, \tag{32}$$

$$\Phi(\mathbf{u}, \nabla\mathbf{u}, \mathbf{x}, t) = 0\,, \tag{33}$$

where $\boldsymbol{u}=(u_1, \ldots, u_K)$ is a vector of unknown functions, eq. (32) describes time evolution and eq. (33) represents either algebraic differential constraints or boundary conditions or elliptic partial differential equations. Such a system of eqs (32) and (33) describes the equations associated with mantle convection and crustal dynamics in which the effects of inertia are small but the advection of temperature can be large. The numerical method is formally derived by evaluating the governing partial differential equations (32) and (33) at collocation points, which results in a system of non-linear ordinary differential algebraic equations describing the evolution of the solution at these collocation points. Spatial derivatives of a function $u_i(x, y, t)$ at collocation points are found using the FWCT.

In order for the algorithm to resolve all the structures appearing in the solution, the basis of active wavelets and, consequently, the computational grid should adapt dynamically in time to reflect local changes in the solution. The adaptation of the computational grid is based on the analysis of wavelet coefficients.

The contribution of a wavelet to the approximation is considerable if and only if the nearby structures of the solution have comparable size to the wavelet scale. Thus, we may drop the large number of fine-scale wavelets with small coefficients in the regions where the solution is smooth. In the wavelet collocation method every wavelet is uniquely associated with a collocation point. Consequently, the collocation point should be omitted from the computational grid if the associated wavelet is omitted from the approximation. This property of the multilevel wavelet approximation allows local grid refinement up to an arbitrary small scale without a drastic increase in the number of gridpoints.

To ensure accuracy of the approximation, the basis should consist of wavelets whose coefficients are or can possibly become significant during the period of time when the basis remains unchanged. Thus, at any instant, the basis should include wavelets belonging to an *adjacent zone* of wavelets for which the magnitudes of the coefficients satisfy criterion (29). We say that the 2-D wavelet $\psi^s_{m,n}(x, y)$ belongs to the adjacent zone of wavelet $\psi^j_{k,l}(x, y)$ if the following relations are satisfied:

$$|j - s| \le L_a\,, \quad |b^j_{xm} - b^s_{xk}| \le M_x a_{xs}\,, \quad |b^j_{yn} - b^s_{yl}| \le M_y a_{ys}\,, \qquad (34)$$

where L_a determines the extent to which coarser and finer scales are included in the adjacent zone and M_x and M_y define the width of the adjacent zone in physical space. The concept of adjacent zones is illustrated in Fig. 3 by showing the adjacent zone of 1-D wavelet ψ^j_k for $L_a = 1$ and $M_x = 1$.

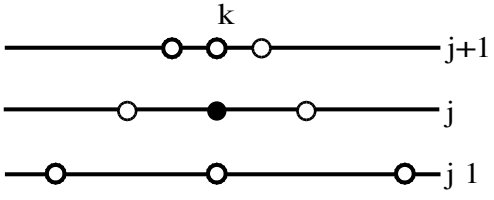

Figure 3. Locations of wavelets (marked with circles) belonging to the adjacent zone of 1-D wavelet ψ^j_k ($L = 1$, $M = 1$).

The values of L_a, M_x and M_y affect the total number of collocation points present in the irregular grid at any instant and the time interval during which the calculations can be carried out without modifying the computational grid. For efficiency we want to keep the number of collocation points as small as possible, while at the same time we would like to minimize changes in the collocation grid.

Let us denote by $\mathcal{G}^t_{\ge}$ the irregular grid of wavelet collocation points that are retained to approximate the solution at time t. Following the classical collocation approach and evaluating eqs (32) and (33) at collocation points (x^J_k, y^J_k) $(k, l) \in Z_{xy\ge}$, we obtain a system of ordinary differential equations.

The present numerical algorithm consists of three steps.

(i) Knowing the values of the solution $\boldsymbol{u}^J_{i,k}(t)$, we compute the values of wavelet coefficients at all levels of resolution. For a given threshold ε we adjust $\mathcal{G}^{t+\Delta t}_{\ge}$ based on the magnitude of wavelet coefficients.

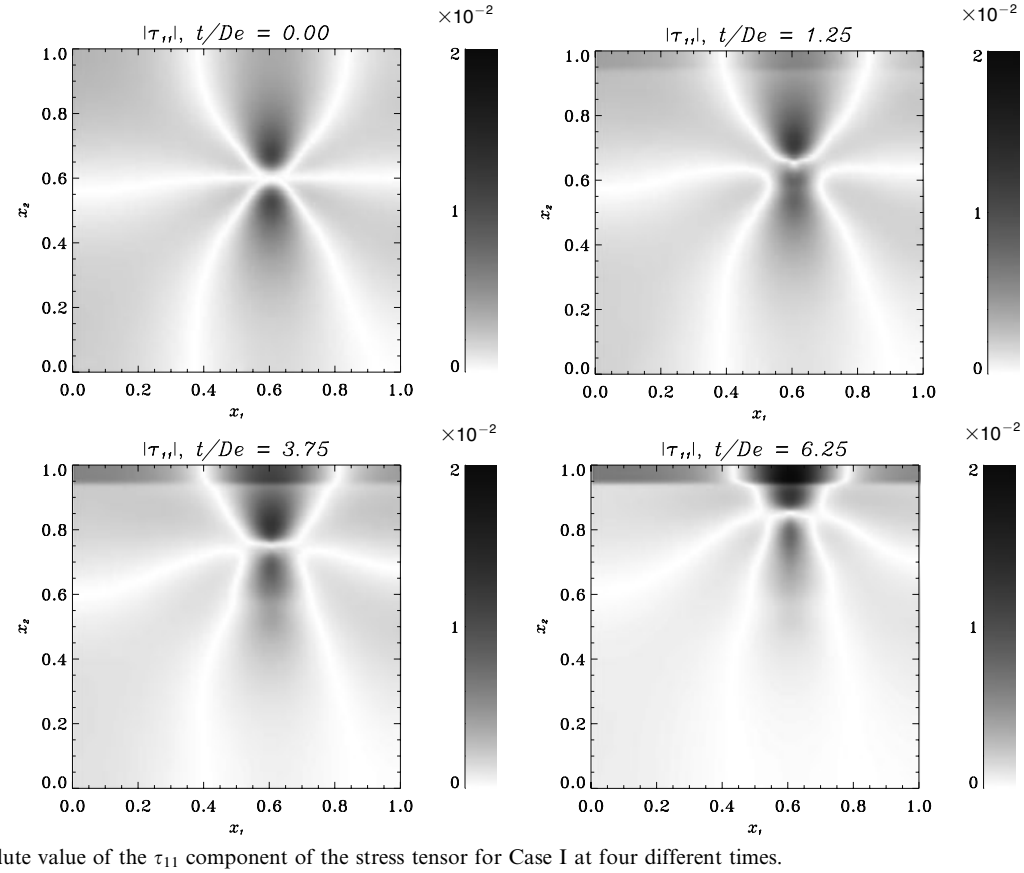

Figure 4. Absolute value of the τ_{11} component of the stress tensor for Case I at four different times.

(ii) If there is no change between computational grids $\mathscr{G}^t_{\geq}$ and $\mathscr{G}^{t+\Delta t}_{\geq}$ at times t and $t+\Delta t$, we go directly to step (iii). Otherwise, we compute the values of the solution at the collocation points $\mathscr{G}^{t+\Delta t}_{\geq}$, which are not included in $\mathscr{G}^t_{\geq}$.

(iii) We integrate the resulting system of ordinary differential equations to obtain new values, $u^J_{i,k}(t+\Delta t)$, at positions on the irregular grid $\mathscr{G}^{t+\Delta t}_{\geq}$ and go back to step (i).

The basic hypothesis motivating the algorithm is that during a time interval Δt, the domain of wavelets with significant coefficients does not move in phase space beyond its border. With such an algorithm the irregular grid of wavelet collocation points is dynamically adapted in time and follows the local structures that appear in the solution. Note that by omitting wavelets with coefficients below a threshold parameter ε, we automatically control the error of approximation. Thus the wavelet collocation method has another important feature: active control of the accuracy of the solution. The smaller the value of ε chosen, the smaller the error of the solution. In typical applications the value of ε varies between 10^{-2} and 10^{-4}. We also note that the larger the value of ε, the fewer the number of gridpoints necessary to obtain the solution.

The results presented in this paper have been obtained by using the threshold parameter $\varepsilon = 5\times10^{-3}$, which means that the local relative error is less than 5×10^{-3} everywhere. The adaptation of the computational grid is based on the analysis of coefficients associated with all six dependent variables of eqs (1)–(3). The irregular grid $\mathscr{G}\geq^t$ of wavelet collocation points is constructed as a union of irregular grids corresponding to each dependent variable.

4 RESULTS AND DISCUSSION

Modelling of mantle flows with sharp viscosity contrasts in a viscoelastic medium is a challenging computational problem in geodynamics because of its multiple-scale nature in the spatio-temporal dynamics and the spatial variability of the local Deborah number due to the strong temperature dependence of mantle viscosity. Because our viscoelastic model is kinematic in nature, that is, the velocity of the rising diapir is prescribed *a priori*, it is rather difficult to make more detailed quantitative comparison with existing models (e.g. Moresi *et al.* 2000). For this reason, we will only concentrate on the results that demonstrate the efficacy of the adaptive wavelet collocation method to capture the sharp gradients of the stress and pressure fields developed during the diapiric impingement process.

The solution for the τ_{11} component of the stress tensor and the corresponding computational grid for Case I are shown in Figs 4 and 5, respectively, for four different times. The build-up of a high stress region in the lithosphere just above the diapir is illustrated in Fig. 4. We coin this phenomenon a *stress-focusing effect*. For physical dimensions and values characteristic of the realistic Earth mantle, the magnitudes of the stress fields

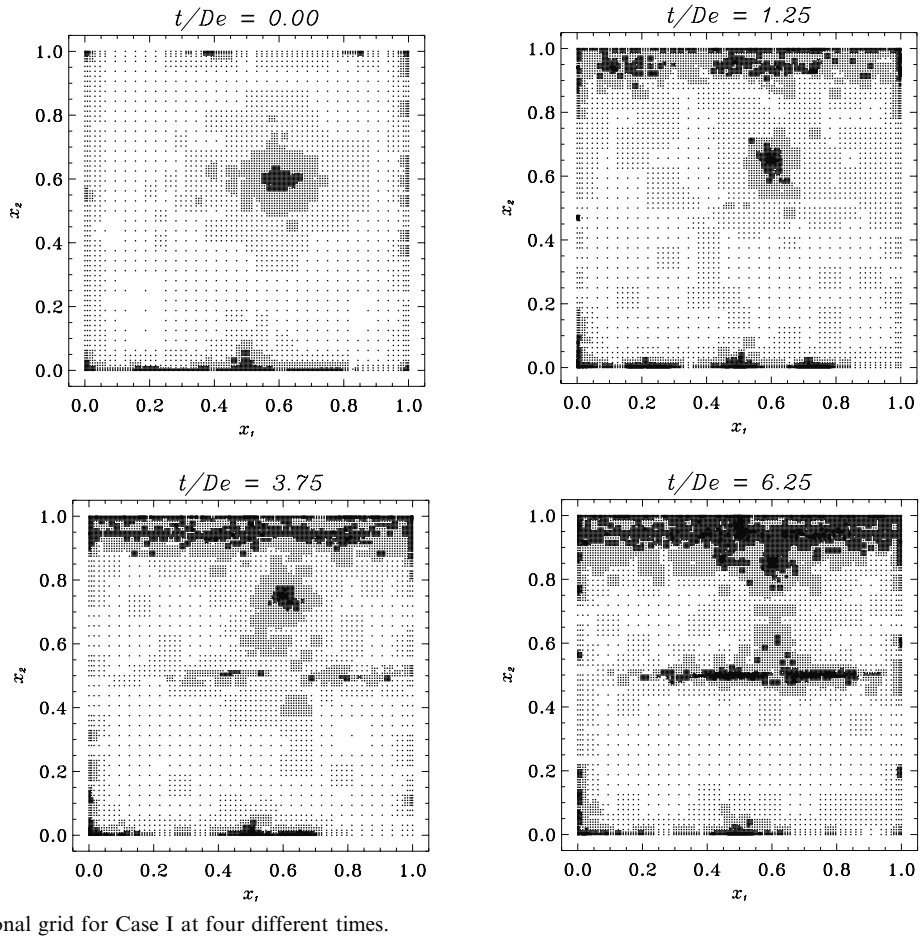

Figure 5. Computational grid for Case I at four different times.

can reach around 100–300 MPa, which are comparable to the values in viscoelastic thermal convection (Moresi *et al.* 2000). These results show that viscoelasticity can play an important role in lithospheric dynamics, especially concerning the potential severage of the lithosphere by mantle plumes.

The capability of the numerical algorithm to resolve localized structures is illustrated in Fig. 5. It is observed that the computational grid is very fine only in the regions where small-scale features or large gradients are present. Note that the total number of collocation points at any instant did not exceed 3×10^4. The same calculation on a non-adaptive regularly spaced 2-D grid with the same resolution using conventional numerical algorithms would require more than 10^6 gridpoints. Thus we have a compression ratio of around 100 in terms of the reduction of gridpoints needed in the wavelet scheme. If one repeats the same calculation on a non-adaptive regularly spaced 2-D grid using conventional numerical algorithms with the same number of gridpoints, i.e. 3×10^4, these results will be inaccurate because of the inadequate spatial resolution for resolving the sharp gradients of the stress fields.

Comparisons of the τ_{11} component of the stress tensor for Cases I–IV are shown in Fig. 6 for approximately the same diapir location. It is clearly seen that the stress-focusing phenomenon is the signature of the lithosphere, the high-viscosity region. The thickness of the lithosphere for Case III is four times less than that for Case II. We also note that the numerical algorithm adapts to the thinning of the lithosphere by increasing resolution only in the region of the lithosphere. Comparison of the results for Cases II and IV illustrates a very important point of the stress-focusing phenomenon. If one looks at the boundary of the high stress, it is located at approximately the same viscosity values. This is because the velocity decreases substantially due to high viscosity. It is not that important whether the viscosity is 10 or 100 times higher; what is important is the viscosity contrast. If one bases the lithosphere thickness on the value of λ, then one should expect to have the same lithosphere thickness. However this is not the case, as is easily seen in the figures. If one bases the definition of thickness on the absolute value of the viscosity, then the lithosphere thickness should be approximately 1.4 times larger for Case IV than for Case II. This is confirmed in Fig. 6.

The elastic effects can be observed by examining the quantity $\tau_{11}+\tau_{22}$, which should be zero in the pure viscous limit. Thus the deviation of this quantity from zero gives us a measure of the degree of elasticity in the stress distribution. The viscoelastic memory effects on the stress distribution are illustrated in Fig. 7, where solutions for τ_{11} and $\tau_{11}+\tau_{22}$ for Case V are shown. This solution has been obtained by setting the rising speed of the diapir velocity to zero and then monitoring the subsequent relaxation. This condition effectively locks the diapir at a fixed position, but the stress distribution then decreases with time from the viscoelastic solution. This process takes a long time, of the order of 10 Maxwell relaxation times.

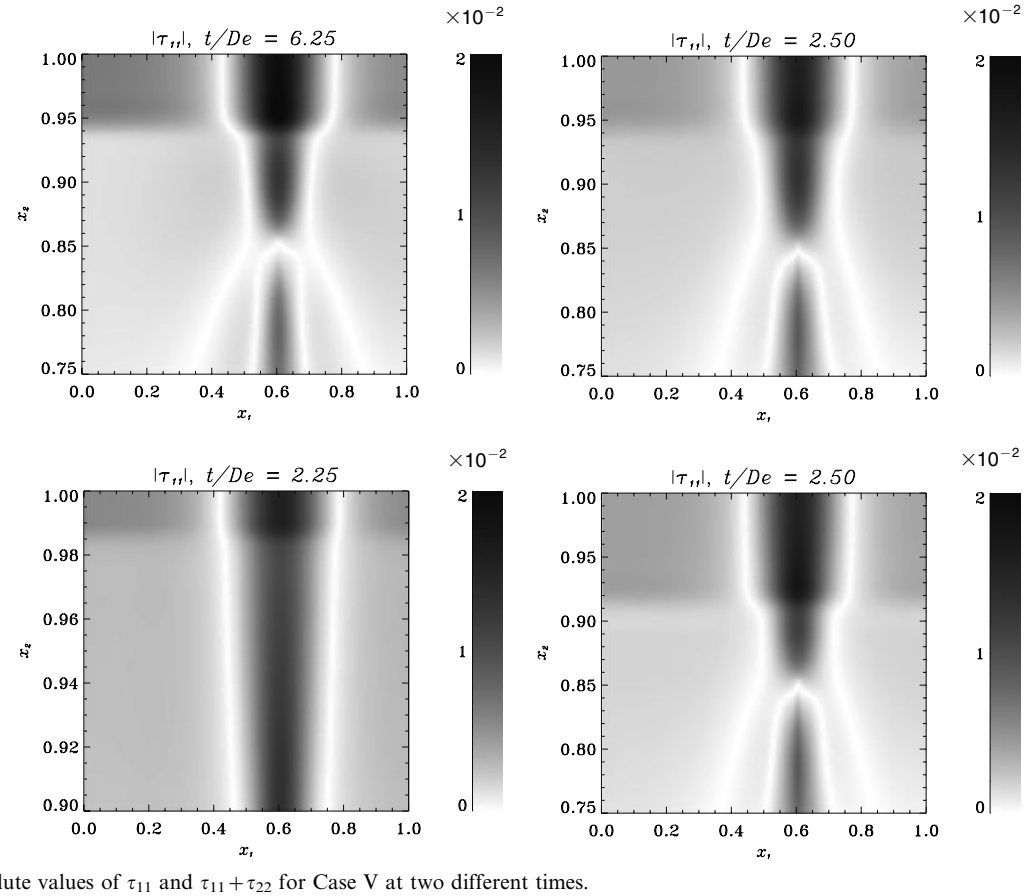

Figure 6. Absolute values of τ_{11} and $\tau_{11}+\tau_{22}$ for Case V at two different times.

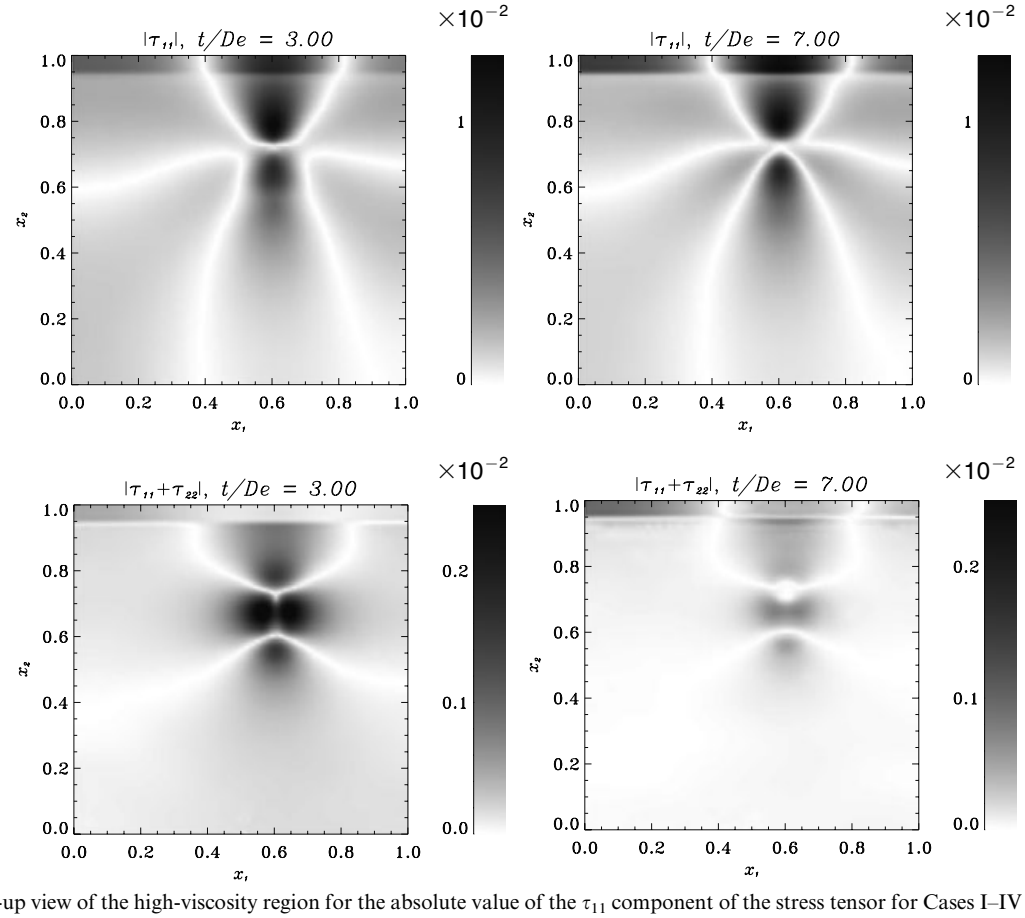

Figure 7. Close-up view of the high-viscosity region for the absolute value of the τ_{11} component of the stress tensor for Cases I–IV of Table 1 for the same diapir location.

5 CONCLUSIONS

In this paper we have demonstrated in 2-D simulations the prowess of the dynamically adaptive wavelet collocation method to approach the regime of realistic mantle lithospheric interaction by considering thin layers, $O(10)$ km, and viscosity contrasts up to 10^8. The multilevel wavelet approximation has allowed for local grid refinement up to an arbitrarily small scale, of the order of 1 km, without a drastic increase in the number of collocation points, about 10^4 in two dimensions. In three dimensions this would be about 10^6 collocation points, which would still be affordable in current computational environments.

We have developed a new wavelet-based method for solving partial differential equations describing viscoelastic diapiric flows with strong localized viscosity variations. We have verified early findings of stress amplification in a thin very viscous layer (Poliakov *et al.* 1993; Podlachikov *et al.* 1993) in that several hundred megaPascals were found to develop in the lithosphere. This raises the possibility of the breaking of the viscoelastic lithosphere by interaction with a rising diapir. With the use of our highly adaptive method, we can model much thinner lithosphere than the more conventional finite difference method used by Poliakov *et al.* (1993) or the finite element scheme of Moresi *et al.* (2000), which had a resolution of around a few kilometres. The wavelet approach will allow us to glean more valuable information on the nature of tectonics and the stress state of the lithosphere under compression or tension. The wavelet method can help to bridge the scales by providing a sharp picture of the detailed mechanics leading to the failure of the lithosphere and the conditions for major failure to occur. This will be the aim of future work, which will entail the adaptation of this method to treat the mechanism of stress advection in the finite amplitude regime (Schmalholz & Podladchikov 1999), to incorporate the thermomechanical effects into situations involving localization (Kameyama *et al.* 1999) and to include a geophysically realistic yield stress criterion (Kohlstedt *et al.* 1995), thus allowing for the possibility of severage of the lithosphere.

ACKNOWLEDGMENTS

We acknowledge fruitful discussions with Arkady Ten and A. Bobby Poliakov. This research has been supported by the geophysics program of the National Science Foundation.

REFERENCES

Braun, J. & Sambridge, M., 1994. Dynamical Lagrangian remeshing (DLR)—a new algorithm for solving large strain deformation problems and its application to fault-propagation folding, *Earth planet. Sci. Lett.*, **124,** 211–220.

Chery, J., Bonneville, A., Vilotte, J.P. & Yuen, D.A., 1991. Numerical modelling of caldera dynamical behaviour, *Geophys. J. Int.*, **105,** 365–379.

Christensen, U.R. & Ribe, N.M., 1994. 3-dimensional modeling of plume-lithosphere interaction, *J. geophys. Res.,* **99,** 669–682.

Daubechies, I., 1992. Ten lectures on wavelets, in *CBMS-NSF Series in Applied Mathematics,* No. 61, SIAM, Philadelphia.

Donoho, D.L., 1992. Interpolating wavelet transforms, *Tech. Rept,* 408, Department of Statistics, Stanford University, CA.

Harder, H., 1991. Numerical simulation of thermal convection with Maxwellian viscoelasticity, *J. Non-Newtonian Fluid Mech.,* **39,** 67–88.

Huilgol, R.R. & Phan-Thien, N., 1997. *Fluid mechanics of visco-elasticity: general principles, constitutive modeling, analytical and numerical techniques,* Elsevier, Amsterdam.

Kameyama, M., Yuen, D.A. & Karato, S., 1999. Thermal-mechanical effects of low-temperature plasticity (the Peierls mechanism) on the deformation of a viscoelastic shear zone, *Earth planet. Sci. Lett.,* **168,** 159–172.

Keunings, R., 2001. Advances in the computer modeling of the flow of polymeric liquids, *Comp. Fluid Dyn. J.,* **9,** 449–458.

Kohlstedt, D.L., Evans, B. & Mackwell, S.J., 1995. Strength of the lithosphere: constraints imposed by laboratory experiments, *J. geophys. Res.,* **100,** 587–602.

Larsen, T.B., Malevsky, A.V., Yuen, D.A. & Smedsmo, J.L., 1993. Temperature-dependent Newtonian and non-Newtonian convection: implications for lithospheric processes, *Geophys. Res. Lett.,* **20,** 2595–2598.

Louis, A.K., Maaß, P. & Rieder, A., 1997. *Wavelets: Theory and Applications,* John Wiley & Sons, New York.

Malevsky, A.V. & Yuen, D.A., 1992. Strongly chaotic non-Newtonian mantle convection, *Geophys. Astrophys. Fluid Dyn.,* **65,** 149–171.

Melosh, H.J. & Raefsky, A., 1980. The dynamical origin of subduction zone topography, *Geophys. J. R. astr. Soc.,* **60,** 333–354.

Meyer, Y., 1992. Wavelets and operators, *Cambridge Studies in Advanced Mathematics,* 37, Cambridge University Press, Cambridge (English Transl. by Salinger, D.H.).

Moresi, L., Dufour, F. & Muhlhaus, H., 2001. Mandle convection models with viscoelastic/brittle lithosphere: Numerical methodology and plate tectonic modeling, *PAGEOPH,* in press.

Podlachikov, Y.Y., Lenardic, A., Yuen, D.A. & Quareni, F., 1993. Dynamical consequences of stress focusing for different rheologies: Earth and Venus perspectives, *EOS, Trans. Am. geophys. Un.,* **74,** 598.

Poliakov, A.N.B., Cundall, P.A., Podlachikov, Y.Y. & Lyakhovsky, V.A., 1993. An explicit inertial method for the simulation of visco-elastic flow, in *Flow and Creep in the Solar System: Observations, Modeling and Theory,* pp. 175–196, eds Stone, D.B. & Runcorn, S.K., Kluwer Academic, Dordrecht.

Reiner, M., 1964. The Deborah number, *Physics Today,* **17,** 62–64.

Ricard, Y., Richards, M., Lithgow-Bertelloni, C. & Le Stunff, Y., 1993. A geodynamic model of mantle density heterogeneity, *J. geophys. Res.,* **98,** 895–909.

Schmalholz, S. & Podladchikov, Y.Y., 1999. Buckling versus folding: importance of viscoelasticity, *Geophys. Res. Lett.,* **26,** 2641–2644.

Schmalholz, S., Podladchikov, Y.Y. & Schmid, D.W., 2001. A spectral/finite difference method for simulating large deformations of heterogeneous, viscoelastic materials, *Geophys. J. Int.,* **145,** 199–208.

Strang, G. & Nguyen, T., 1996. *Wavelets and Filter Banks,* Wellesley-Cambridge Press, Wellesley, MA.

Sweldens, W. & Schröder, P., 1996. Building your own wavelets at home, in *Wavelets in Computer Graphics,* pp. 15–87, ACM SIGGRAPH Course Notes.

Toth, J. & Gurnis, M., 1998. Dynamics of subduction initiation at preexisting fault zones, *J. geophys. Res.,* **103,** 18 053–18 067.

Vasilyev, O.V., 1996. Multilevel wavelet collocation methods for solving partial differential equations, *PhD thesis,* University of Notre Dame, Notre Dame, IN.

Vasilyev, O.V., 2001. Solving multi-dimensional evolution problems with localized structures using second generation wavelets, *Int. J. Comp. Fluid Dyn.,* in press.

Vasilyev, O.V. & Bowman, C., 2000. Second generation wavelet collocation method for the solution of partial differential equations, *J. Comput. Phys.,* **165,** 660–693.

Vasilyev, O.V. & Paolucci, S., 1996. A dynamically adaptive multilevel wavelet collocation method for solving partial differential equations in a finite domain, *J. Comput. Phys.,* **125,** 498–512.

Vasilyev, O.V. & Paolucci, S., 1997. A fast adaptive wavelet collocation algorithm for multi-dimensional PDEs, *J. Comput. Phys.,* **125,** 16–56.

Vasilyev, O.V., Yuen, D.A. & Paolucci, S., 1997a. The solution of PDEs using wavelets, *Comput. Phys.,* **11,** 429–435.

Vasilyev, O.V., Yuen, D.A. & Podladchikov, Y.Y., 1997b. Applicability of wavelet algorithm for geophysical viscoelastic flow, *Geophys. Res. Lett.,* **24,** 3097–3100.